Timing of Epimerization and Condensation Reactions in Nonribosomal Peptide Assembly Lines: Kinetic Analysis of Phenylalanine Activating Elongation Modules of Tyrocidine Synthetase B†

Lusong Luo,‡ Rahul M. Kohli,‡ Megumi Onishi,‡ Uwe Linne,§ Mohamed A. Marahiel,§ and Christopher T. Walsh*,‡

Department of Biological Chemistry and Molecular Pharmacology, Harvard Medical School, 240 Longwood Avenue, Boston, Massachusetts 02115, and Biochemie/Fachbereich Chemie, Philipps-Universität Marburg, Hans-Meerwein Strasse, D-35032 Marburg, Germany

Received April 30, 2002; Revised Manuscript Received May 28, 2002

ABSTRACT: The cyclic decapeptide antibiotic tyrocidine has D-Phe residues at positions 1 and 4, produced during peptide chain growth from L-Phe residues by 50 kDa epimerase (E) domains embedded, respectively, in the initiation module (TycA) and the $TycB_3$ module of the three-subunit (TycABC), 10-module nonribosomal peptide synthetase. While the initiation module clearly epimerizes the aminoacyl thioester Phe_1-S-TycA intermediate, the timing of epimerization versus peptide bond condensation at internal E domains has been less well characterized in nonribosomal peptide synthetases. In this study, we use rapid quench techniques to evaluate a three-domain (ATE) and a four-domain version (CATE) of the $TycB_3$ module and a six-domain fragment (ATCATE) of the $TycB_{2-3}$ bimodule to measure the ability of the E domain in the $TycB_3$ module to epimerize the aminoacyl thioester Phe-S-$TycB_3$ and the dipeptidyl-S-enzyme (L-Phe-L-Phe-S-$TycB_3$ ⇔ L-Phe-D-Phe-S-$TycB_3$). The chiralities of the Phe-S-enzyme and Phe-Phe-S-enzyme species over time were determined by hydrolysis and chiral TLC separations, allowing for the clear conclusion that epimerization in the internal $TycB_3$ module occurs preferentially on the peptidyl-S-enzyme rather than the aminoacyl-S-enzyme, by a factor of about 3000/1. In turn, this imposes constraints on the chiral selectivity of the condensation (C) domains immediately upstream and downstream of E domains. The stereoselectivity of the upstream C domain was shown to be L-selective at both donor and acceptor sites ($^{L}C_{L}$) by site-directed mutagenesis studies of an E domain active site residue and using the small-molecule surrogate D-Phe-Pro-L-Phe-*N*-acetylcysteamine thioester (D-Phe-Pro-L-Phe-SNAC) and D-Phe-Pro-D-Phe-SNAC as donor probes.

Nonribosomal peptide synthetases (NRPS) carry out the biosynthesis of many pharmacologically important peptide natural products, including vancomycin, bleomycin, cyclosporin, and penicillin precursors in bacteria and fungi (*1*−*3*). A prototypical NRPS system consists of sets of protein modules that function as an assembly line for amino acid selection, activation, loading, and coupling. The order of the modules determines the sequence of the peptide product. The most upstream module functions in chain initiation, the most downstream in chain termination, and all the rest in NRP chain elongation (*4*). Initiation modules (AT) tend to have two core domains, adenylation (A) and thiolation (T), to produce the aminoacyl-AMP and then covalently tether it to the terminal thiol of the pantetheinyl arm of the thiolation domain. All elongation modules (CAT) in addition have condensation (C) domains to carry out peptide bond condensation during chain growth. The termination module will have a CAT core and then a thioesterase (Te) domain to release the full-length chain from its covalent attachment to the assembly line.

In addition to these core NRPS domains, auxiliary domains that can modify the growing peptide chain, such as *N*-acylation, *N*-methylation, and epimerization domains, have also been found embedded, both in initiation and elongation modules (*5*, *6*). The 50 kDa epimerization (E) domains are of particular interest, acting within a module to epimerize the amino acid selected by that module from L to D configuration. The presence of such D-amino acid residues is a hallmark of nonribosomal peptides, creating architectural diversity, providing resistance to proteolysis, and imposing

† This work has been supported by the National Institutes of Health (Grant GM20011 to C.T.W.) U.L. and M.A.M. are supported by the Fonds der chemischen Industrie and the Deutsche Forschungsgemeinschaft.

* To whom correspondence should be addressed: Phone: (617) 432-1715. Fax: (617) 432-0438. E-mail: christopher_walsh@hms.harvard.edu.

‡ Harvard Medical School.

§ Philipps-Universität Marburg.

[1] Abbreviations: NRPS, nonribosomal peptide synthetase; Tyc, tyrocidine; TycA, tyrocidine synthetase A; TycB, tyrocidine synthetase B; L-Phe, L-phenylalanine; Ppant, 4′-phosphopantetheine; aa-S-Ppant-T, aminoacylated thioester form of cofactor Ppant-modified holo T domain; A, adenylation domain; T, thiolation domain; E, epimerization domain; C, condensation domain; ATE, adenylation−thiolation−epimerization domains; Te, thioesterase domain; L-Phe-AMP, L-phenylalanyl-adenosine-5′-phosphate diester; AMP, adenosine 5′-monophosphate; ATP, adenosine 5′-triphosphate; Hepes, N-(2-hydroxyethyl)piperzine-N′-2-ethanesulfonic acid; CoA or CoASH, coenzyme A; NAC, *N*-acetylcysteamine; DIPCDI, diisopropylcarbodiimide; HOBt, hydroxybenzotriazole; IPTG, isopropyl β-D-thiogalactopyranoside; HPLC, high-performance liquid chromatography; LSC, liquid scintillation counting; TCEP, tris-(2-carboxyethyl)phosphine; TCA, trichloroacetic acid; TLC, thin-layer chromatography; MALDI-TOF MS, matrix-assisted laser desorption ionization time-of-flight mass spectrometry.

10.1021/bi026047+ CCC: $22.00
Published on Web 06/26/2002

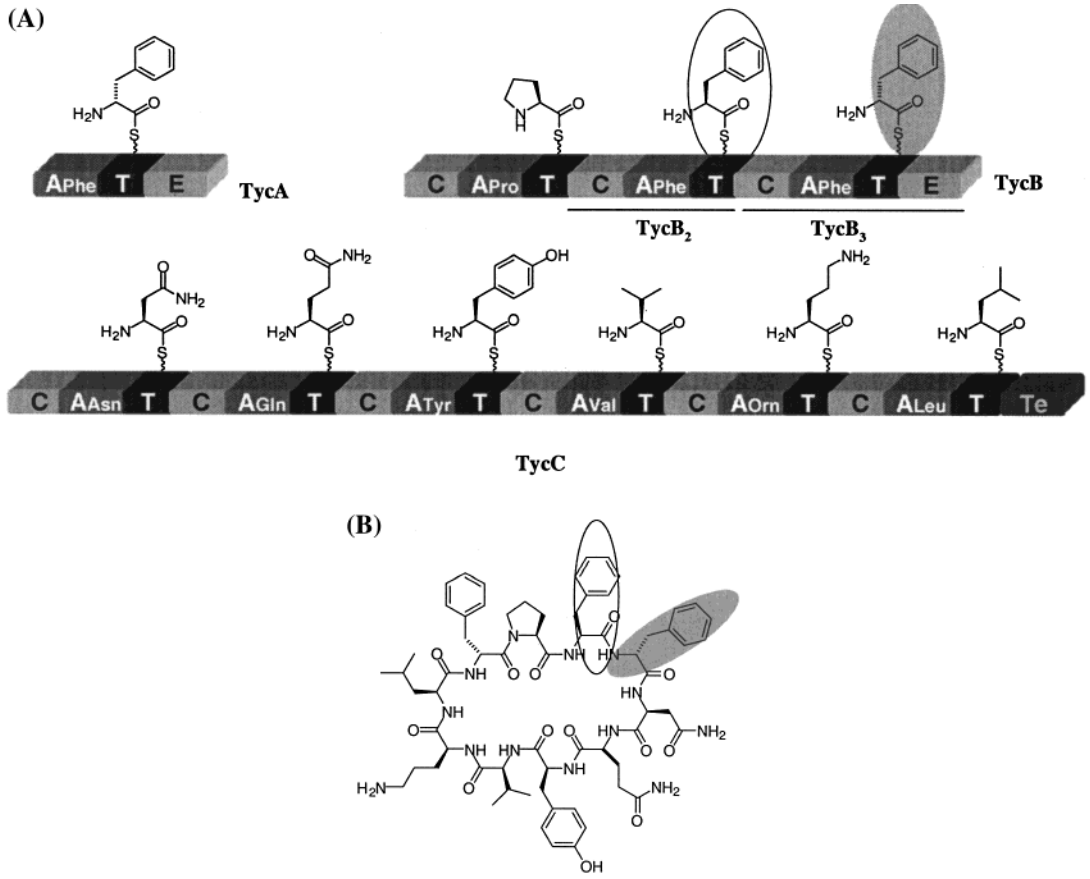

FIGURE 1: Biosynthesis of the cyclodecapeptide antibiotic tyrocidine by the tyrocidine synthetase, a prototypic NRPS. (A) Schematic representation of the 3-subunit (TycA, TycB, and TycC), 10-module and 32-domain Tyc assembly line. The wavy line represents the phosphopantetheine arm of the T domain. (B) The chemical structure of cyclodecapeptide tyrocidine. The L-Phe_3 residue incorporated by $TycB_2$ module is circled, and the D-Phe_4 residue incorporated through *in situ* epimerization by the E domain in the $TycB_3$ module is shaded in the scheme and the chemical structure.

stereochemical constraints (e.g., for the formation of cyclic peptide antibiotic tyrocidine, a D-Phe_1 residue is required for the regio- and stereospecific cyclization of the decapeptidyl intermediate by the Te domain; *7*).

We have previously studied the three domain ATE initiation module of gramicidin synthetase in some detail (*8*−*10*), proving that the Phe-S-T aminoacyl-S-enzyme intermediate is the substrate for *in cis* E domain action. The tyrocidine synthetase (Figure 1) ATE initiation module is highly homologous and likely to follow the same mechanism. On the other hand, the D-Phe_4 residue of the cyclic decapeptide tyrocidine, put in by the $TycB_3$CATE elongation module, could be epimerized analogously as the Phe-S-T_3 aminoacyl thioester before condensation by the C domain or could be epimerized as the D-Phe_1-L-Pro_2-L-Phe_3-L-Phe_4-S-T_3 enzyme intermediate after condensation (Figure 2). Initial steady-state kinetic studies have favored the latter alternative (*11*) for the $TycB_3$ module. Since the timing of E domain versus upstream and downstream C domain action in NRPS assembly lines has strong implications both for coupling of epimerization to peptide chain elongation and the chiral selectivity of C domain catalysts that flank all internal E domains, we have addressed the issue directly with transient kinetic analysis. We started with the three-domain ATE fragment of $TycB_3$ to compare with the GrsA ATE initiation module and then assessed the effects of adding the C domain in the CATE four domain $TycB_3$ module. By addition of two immediately upstream domains, the AT of $TycB_2$ (Figure 1), the six-domain bimodule protein fragment, ATCATE, can be assayed for Phe−Phe dipeptidyl-S-enzyme formation and for epimerization rates on the second Phe before and after the condensation step.

EXPERIMENTAL PROCEDURES

General. L-Phe-L-Phe, L-Phe-D-Phe, D-Phe-L-Phe, and D-Phe-D-Phe dipeptide standards were purchased from Research Plus Inc. *N*-Acetylcysteamine (NAC), tris-(2-carboxyethyl)phosphine (TCEP), diisopropylcarbodiimide (DIPCDI), hydroxybenzotriazole (HOBt), and Boc-protected amino acids were purchased from Aldrich. Radiolabeled L-[^{14}C]Phe (450 mci/mmol) and D-[^{14}C]Phe (56 mci/mmol) were purchased from NEN. Priming of the apo-enzyme (generation of holo-enzyme) was achieved by incubation with CoASH and *Bacillus subtilis* Ppant transferase Sfp (*12*, *13*). Reaction mixtures in assay buffer containing 70 μM apo-enzyme, 250 μM CoASH and 50 nM Sfp were incubated for 60 min at 37 °C. Equilibrium fluorescence measurements were carried out at 25 °C using a PTI Fluorescence System (MD-5020 Motor Driver, LPS-220B Lamp Power Supply, 814 Photomultiplier Detection System). Phosphorimages of TLC plates were obtained after 12 to 36 h exposure to "BAS-MS2040" or "BAS-TR2040" image plates and read by a "Bio-Imaging Analyzer BAS1000" (Fuji). MALDI-TOF mass spectrometry was carried out using a PerSeptive Biosystems Voyager-DE STR mass spectrometer. Analytical HPLC was carried out on a Beckman Gold Nouveau system.

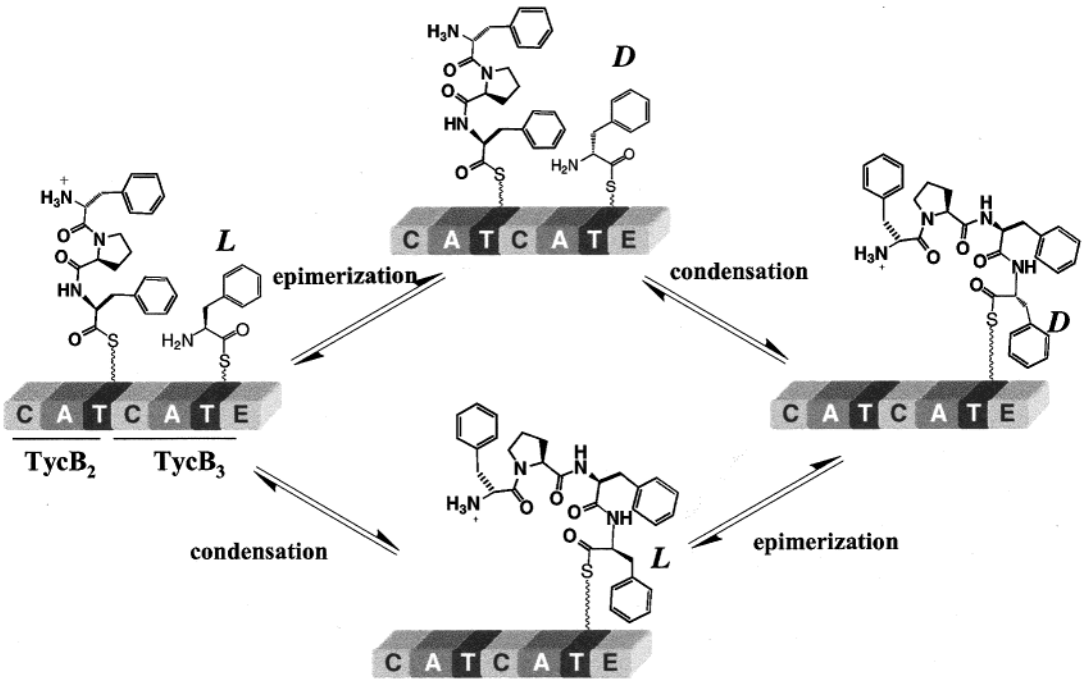

FIGURE 2: Two possible chemical pathways for epimerization and condensation reactions during the peptide elongation by $TycB_2$ and $TycB_3$ modules: upper route, epimerization before condensation; lower route, epimerization after condensation.

Overexpression and Purification of TycB3ATE, TycB3CATE, and TycB2–3ATCATE Proteins. The expression vectors pQE70 (Qiagen) containing $TycB_3$ATE, $TycB_3$CATE, and $TycB_{2-3}$ATCATE genes were transformed into *Escherichia coli*/M15 electrocompetent cells. The cell culture was grown in LB medium (10 mM $MgCl_2$, 100 μg/mL ampicillin and 25 μg/mL kanamycin) at 37 °C to an OD_{600} of 0.6 and induced with 1 mM isopropyl β-D-thiogalactopyranoside (IPTG) for additional 4 h at 25 °C. Cells from 4 × 1 L media were harvested and disrupted as previously described in (*14*). The proteins were purified after single-step Ni^{2+}-affinity chromatography. The fractions containing pure protein judged by SDS−PAGE analysis were dialyzed into 50 mM K^+Hepes buffer (pH 7.5, 1 mM tris-(2-carboxyethyl)-phosphine (TCEP)) and stored at −80 °C. The yield for the three constructs were ca. 5 mg/L.

Determination of Amino Acid Binding Constants by Fluorescence Titration. All fluorescence titration experiments were carried out using a PTI Fluorescence System as previously reported (*8*). The excitation wavelength was 280 nm and the emission spectra were recorded in the range of 300−420 nm for 3 mL solutions containing 0.05 μM enzyme and 0−70 μM L-Phe or D-Phe in 50 mM K^+Hepes buffer (pH 7.5). The observed fluorescence at 327 nm was plotted vs the amino acid concentration and the curve analyzed with eq 1 using the KaleidaGraph computer program:

$$\Delta F_{obs} = \Delta F_{max}/(1 + K_d/[S]) \quad (1)$$

In eq 1, ΔF_{obs} = observed change in fluorescence, ΔF_{max} = the total change in fluorescence, K_d = the apparent dissociation constant of the ligand, and [S] = concentration of the amino acid ligand.

Synthesis of D-*Phe-Pro*-L-*Phe-SNAC,* D-*Phe-Pro*-D-*Phe-SNAC,* D-*Phe-Pro*-L-*Phe*-L-*Phe, and* D-*Phe-Pro*-L-*Phe*-D-*Phe.* Peptide synthesis was carried out on a PerSeptive Biosystems 9050 synthesizer (0.3 mmol scale) using diisopropylcarbodiimide (DIPCDI)/ hydroxybenzotriazole (HOBt) chemistry on 2-chlorotrityl resin. Fmoc-protected monomers (Novabiochem) were used except for the N-terminal D-Phe of the tripeptide, which was Boc-protected. A mixture of 1:1:3 acetic acid/trifluoroethanol/CH_2Cl_2 was used to cleave the peptides from the resin (3 h, 24 °C). The resin was then removed by filtration, the peptides precipitated with *n*-hexane, and the solvent removed by rotary evaporation. For D-Phe-Pro-L-Phe-SNAC and D-Phe-Pro-D-Phe-SNAC formation, the protected tripeptide was dissolved in THF and thioester formation initiated by addition of dicyclohexylcarbodiimide (2 equiv), HOBt (2 equiv), and *N*-acetylcysteamine (10 equiv). After stirring for 1 h (24 °C), K_2CO_3 (0.6 equiv) was added, and the reaction mixture was stirred for an additional 3 h. The reaction mixture was then filtered and the solvent removed by rotary evaporation. Deprotection of the N-terminal Boc was carried out using TFA with triisoproylsilane (2.5%) and water (2.5%) for 3 h at 24 °C. The solvent was evaporated, and the product was dissolved in 20% DMSO in water and filtered. The peptide thioester was purified by preparative HPLC with a reversed-phase C_{18} column, using a gradient from 10% to 50% acetonitrile in 0.1%TFA/water over 60 min. Lyophilization afforded the peptide−SNAC as a white powder. The identity and purity of the peptide thioester and peptide acids were confirmed by analytical HPLC and MALDI-TOF mass spectrometry.

Construction and Purification of $TycB_{2-3}$ ATCATE H1773A Mutant. Plasmid of H1773A mutant was created by SOE mutagenesis (*15*) of the wild-type $TycB_{2-3}$ ATCATE plasmid pATCATE using the following oligonucleotides (the Ala codon is highlighted in bold): $TycB_{2-3}$ ATCATEout5′F, 5′-GCTATTGGAATCGTCCAGAGCTGAC-3′; H1773A5′F, 5′-GTCGCGATCCAC**GCG**CTTGTCGTGGATGGC-3′; H1773A3′B, 5′-GCCATCCACGACAAG**CGC**GTGGATCGC-GAC-3′; $TycB_{2-3}$ ATCATEout3′B, 5′- CAAATCCAGATG-GAGTTCTGAGGTC-3′. The amplification product was

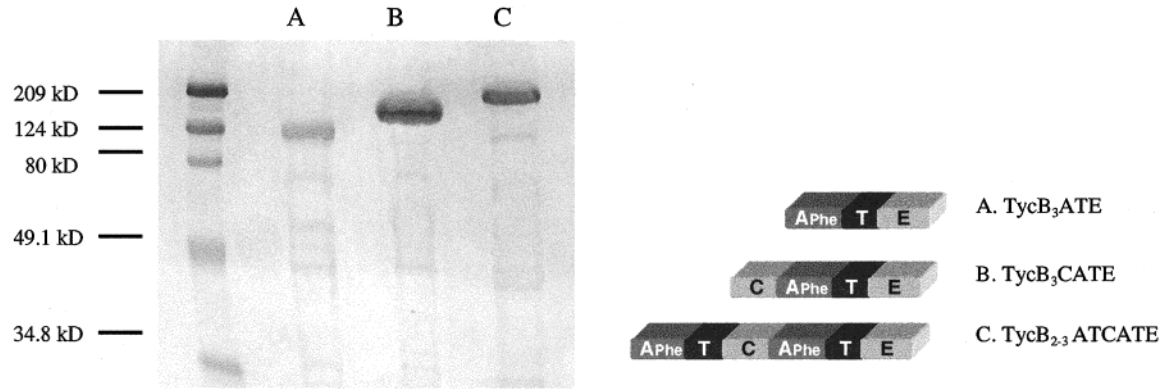

FIGURE 3: 12% SDS−PAGE gel showing purified $TycB_3ATE$, $TycB_3CATE$, and $TycB_{2-3}ATCATE$.

Table 1: Dissociation Constants for Binding of L-Phe and D-Phe to the Adenylation Domain of $ApoTycB_3ATE$, $ApoTycB_3CATE$, and $ApoTycB_{2-3}ATCATE$

	K_d (μM)	
amino acid	L-Phe	D-Phe
$apoTycB_3ATE$	3.4 ± 0.4	6.0 ± 0.3
$apoTycB_3CATE$	5.0 ± 0.6	2.6 ± 0.2
$apoTycB_{2-3}ATCATE$	4.2 ± 0.5	6.7 ± 1.3

digested by *Sna*B I and *Bam*H I restriction enzymes and ligated to the complementing product of similarly digested wild-type pATCATE plasmid. The ligation product was transformed to *E. coli* DH5α, and the identity of the mutant was confirmed by DNA sequencing at the Molecular Biology Core Facilities of the Dana Farber Cancer Institute. Expression and purification of the His_6-tagged H1773A mutant was performed as previously described (*14*), except that *E. coli* DH5α was used as the host cell for overexpression. Overproduction and purification after single-step Ni^{2+}-affinity chromatography was confirmed by SDS−PAGE analysis. The purified H1773A fraction was dialyzed into 50 mM K^+Hepes buffer (pH 7.5, 1 mM TCEP) and stored at −80 °C. The yield for H1773A purification was ca. 3 mg/L.

Measurement of Single-Turnover Time Courses Using the Rapid-Quench Flow Apparatus. Single-turnover time courses for reactions catalyzed by apo- and holo-enzymes were measured in manners similar to those described in refs *8* and *10*. All reactions finished within 300 s were carried out at 30 °C using a rapid-quench flow apparatus from KinTek instruments. Reactions with time points longer than 300 s were hand-quenched instead of using the rapid-quench flow apparatus. The final concentrations after mixing (total volume 30 μL) were typically 35 μM enzyme, 5 μM L-[^{14}C]Phe or D-[^{14}C]Phe, 5 mM $MgCl_2$, 4 mM ATP, and 0.5 mM TCEP (for the $holoTycB_3CATE$ reaction, 500 μM D-Phe-Pro-L-Phe-SNAC or D-Phe-Pro-D-Phe-SNAC was added to serve as the donor substrate for condensation reaction). The reaction mixture was quenched with 100 μL 10% TCA (w/v) after incubation for a specified period of time. All quench solutions were collected in a 2 mL Eppendorf tube. Following vigorous vortexing, the precipitated protein was pelleted by centrifugation for 20 min at 11 600 g at 4 °C. The separation of radiolabeled amino acid and aminoacyl-AMP in the supernatant was achieved by cellulose TLC (developing buffer A: 4:1:1 (v/v) butanol/water/acetic acid). The separation of L-[^{14}C]Phe and D-[^{14}C]Phe hydrolyzed from the pellet was achieved by chiral TLC (developing buffer B: 4:1:1 (v/v) acetonitrile/water/methanol). For $holoTycB_{2-3}ATCATE$ and H1773A reactions, the radiolabeled L-Phe, D-Phe, L-Phe-L-Phe, L-Phe-D-Phe, D-Phe-L-Phe, and D-Phe-D-Phe were applied to both chiral TLC (developing buffer B) and silica TLC (developing buffer C: 1:1:1:1 (v/v) acetic acid/water/butanol/ethyl acetate). For the $holoTycB_3CATE$ reaction, the L-Phe, D-Phe, D-Phe-Pro-Phe-L-Phe, and D-Phe-Pro-Phe-D-Phe hydrolyzed from the enzyme were analyzed by both chiral TLC assay (developing buffer B) and silica TLC assay (developing buffer B). The microscopic kinetic rate constants of apo-enzyme reactions were obtained by fitting the single-turnover progress curve data to the enzymatic mechanistic scheme (eq 2) using the program DYNAFIT by Petr Kuzmic (*16*). The apparent first-order rate constants were determined by fitting the experimental data to eq 3 using the KaleidaGraph nonlinear regression computer program

$$\text{apoPheATE}\cdot\text{a.a}\cdot\text{ATP}\cdot Mg^{2+} \underset{k_{-1}}{\overset{k_1}{\rightleftharpoons}} \text{apoPheATE}\cdot\text{a.a-AMP}\cdot\text{PPi}\cdot Mg^{2+} \quad (2)$$

$$[P]_t = [P]_{max}(1 - \exp(-kt)) \quad (3)$$

In eq 3, $[P]_t$ = product formation at time t, $[P]_{max}$ = maximal product formation, and k = apparent first-order rate constant.

The single-module $holoTycB_3ATE$ and $holoTycB_3CATE$ reaction data were fitted to enzymatic mechanistic scheme (eq 4) using the program DYNAFIT (*16*)

$$\begin{aligned} &\text{HoloTycB}_3\text{ATE}\cdot\text{L-Phe.ATP}\cdot Mg^{2+} \underset{k_{-1}}{\overset{k_1}{\rightleftharpoons}} \\ &\qquad \text{HoloTycB}_3\text{ATE}\cdot\text{L-Phe-AMP}\cdot Mg^{2+}\cdot\text{PPi} \\ &\underset{k_{-2}}{\overset{k_2}{\rightleftharpoons}} \begin{matrix}\text{L-Phe}\\ |\\ \text{HoloTycB}_3\text{ATE}\end{matrix} \underset{k_{-3}}{\overset{k_3}{\rightleftharpoons}} \begin{matrix}\text{D-Phe}\\ |\\ \text{HoloTycB}_3\text{ATE}\end{matrix} \end{aligned} \quad (4)$$

RESULTS

Overproduction, Purification, and Substrate Binding Characterization of $TycB_3ATE$, $TycB_3CATE$, and $TycB_{2-3}ATCATE$. The 124 kDa $TycB_3ATE$, 169 kDa $TycB_3CATE$, and 238 kDa $TycB_{2-3}ATCATE$ derived from module 2 and/or module 3 of tyrocidine synthetase B (*11*) were overexpressed and purified (Figure 3). To determine the dissociation constants (K_d) of L-Phe and D-Phe to the adenylation domains in each

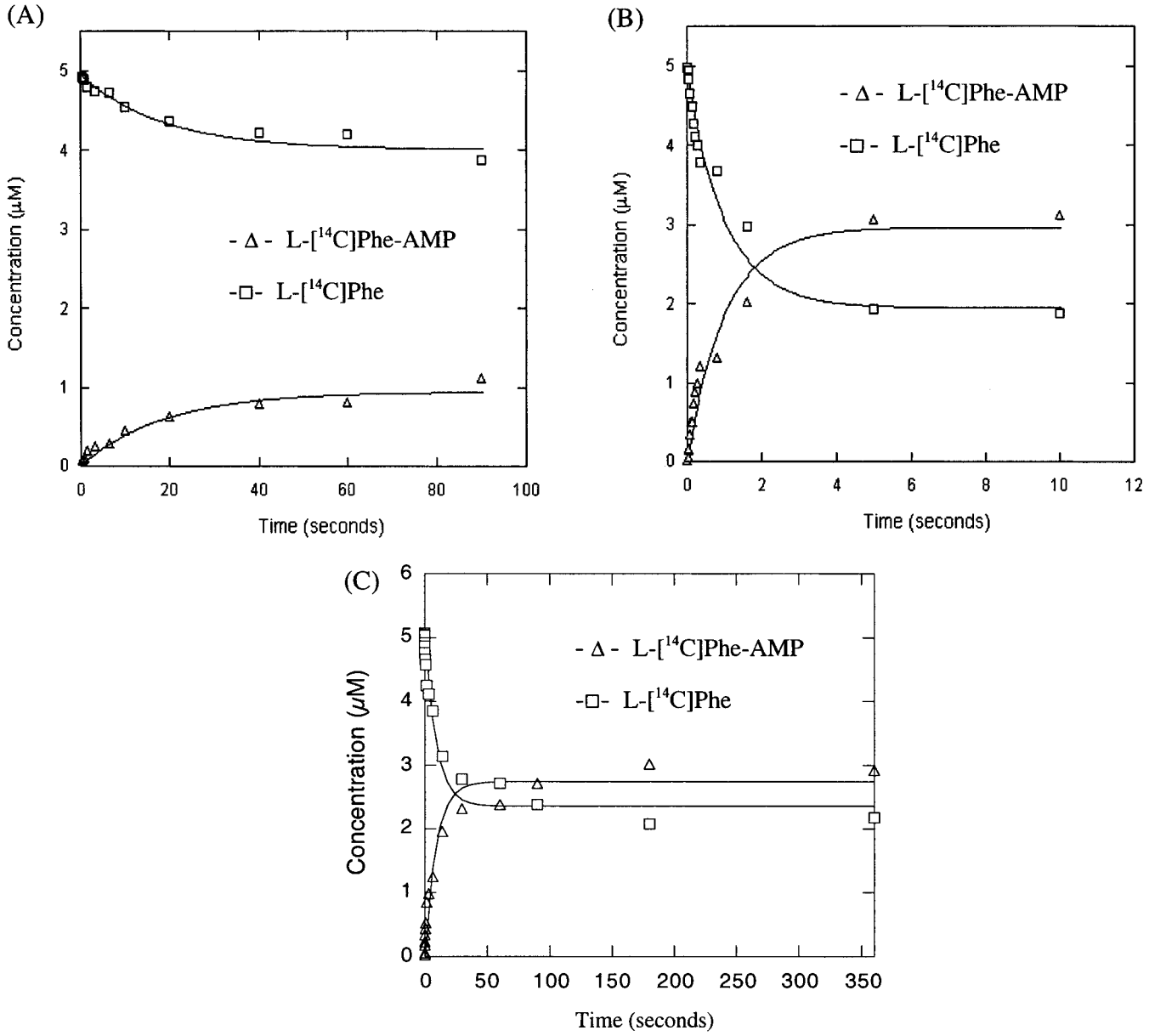

FIGURE 4: Time courses for the single-turnover reactions of 35 μM (A) apoTycB$_3$ATE, (B) apo TycB$_3$CATE, and (C) apo TycB$_{2-3}$ ATCATE with 5 μM L-[^{14}C]Phe, 5 mM $MgCl_2$, 4 mM ATP, and 0.5 mM TCEP in 50 mM K^+Hepes (pH 7.5). The L-[^{14}C]Phe (□) and L-[^{14}C]Phe-AMP (△) are shown with progress curves fitted by DYNAFIT.

construct, we employed the equilibrium fluorescence titration method as previously described (*8*). The K_d values obtained are shown in Table 1. For all three protein constructs, the dissociation constants measured using equilibrium fluorescence titration method ranged from 3 to 7 μM regardless of the chirality of the substrate. These results were in good agreement with that observed in the study of A domain of the gramicidin S synthetase initiation module PheATE (GrsA) (*8*). For GrsA, the K_d values of L-Phe and D-Phe to the L-Phe activating A domain were 6 and 7 μM, respectively. The very similar K_d values obtained for L-Phe and D-Phe to three different L-Phe activating A domains in TycB$_{2-3}$ATCATE (TycB$_2$A$_2$ and TycB$_3$A$_3$) and GrsA (A$_1$) constructs indicated that the L-Phe specific A domains in those constructs can accommodate both stereoisomers equally well. The fluorescence titration curves of both L-Phe and D-Phe to TycB$_{2-3}$ATCATE appeared to resemble that of TycB$_3$ATE and TycB$_3$CATE (data not shown) despite the presence of two A domains in the TycB$_{2-3}$ATCATE, indicating that these two A domains may behave similarly in substrate binding.

L-Phe-AMP Formation by Apo-Enzyme under Single-Turnover Reaction Conditions. To determine the transient kinetic rates of L-Phe-AMP formation within the active site of A domains in the three constructs, we carried out single-turnover analyses using a rapid-quench apparatus following the procedures previously reported (*10*). For the quench reactions, 35 μM apo-enzyme was acid-quenched after exposure to 4 mM ATP and 5 μM L-[^{14}C]Phe for specified periods of time. At these concentrations, 81−88% of free L-[^{14}C]Phe will be enzyme-bound, according to the K_d values measured by fluorescence titration, validating the single-turnover status of the reactions. The profiles for single-turnover reactions of apoTycB$_3$ATE, apoTycB$_3$CATE, and apoTycB$_{2-3}$ATCATE with L-Phe are shown in Figure 4, and the rate constants and apparent internal equilibrium constants are listed in Table 2. Comparisons of rate constants for L-Phe-AMP formation by apoTycB$_3$ATE ($k_1 = 0.01$ s^{-1}, $k_{-1} = 0.04$

Table 2: Rate Constants for Aminoacyl-AMP Formation Catalyzed by ApoTycB$_3$ATE, ApoTycB$_3$CATE, and ApoTycB$_{2-3}$ATCATE

protein construct	k_{eq}^{app} [a]	k_1 (s^{-1})	k_{-1} (s^{-1})	k_1^{app} [b]
apoPheATE (GrsA)[c]	2	2.2 ± 0.1	1.1 ± 0.1	3.1 ± 0.3
apoTycB$_3$ATE	0.23	0.01 ± 0.001	0.044 ± 0.007	0.06 ± 0.01
apoTycB$_3$CATE	1.5	0.58 ± 0.05	0.38 ± 0.05	1.0 ± 0.1
apoTycB$_{2-3}$ATCATE	1.3			0.11 ± 0.01

[a] Apparent internal equilibrium constant = [aminoacyl-AMP]/[amino acid] measured from the ratio of the two species at equilibrium. [b] k_1^{app} values were obtained by fitting the data to single-exponential eq 3. [c] GrsA results were reported in ref *10*.

s^{-1}) and apoTycB$_3$CATE ($k_1 = 0.58\ s^{-1}$, $k_{-1} = 0.38\ s^{-1}$) to that of apoGrsA ($k_1 = 2.2\ s^{-1}$, $k_{-1} = 1.1\ s^{-1}$, reported in ref *10*) showed that the three-domain apoTycB$_3$ATE was significantly slower than apoTycB$_3$CATE and apoGrsA in L-Phe-AMP formation. ApoTycB$_3$ATE has reduced ability to stabilize the L-Phe-AMP intermediate, as judged by the internal equilibrium constants. On the other hand, the rate constants and internal equilibrium constants of the four-domain apoTycB$_3$CATE are comparable to that of apoGrsA. These results suggested that the N-terminal C domain might be structurally important for the proper functioning of the adjacent A domain in the CATE module. There are two adenylation domains in the apoTycB$_{2-3}$ATCATE construct, complicating the determination of the microscopic rate constants. The apparent first-order rate constants obtained by fitting the data to single-exponential equation showed that the apoTycB$_{2-3}$ATCATE has a L-Phe-AMP formation rate on the same order as that of the apoTycB$_3$CATE reaction.

Characterization of Single-Turnover Reactions Catalyzed by HoloTycB$_3$ATE and HoloTycB$_3$CATE. The transient kinetic characterization of adenylation, thiolation, and epimerization reactions catalyzed by holoTycB$_3$ATE and holoTycB$_3$CATE enzyme modules was built on much of the previous efforts toward investigation of the holoGrsA reactions (*8*, *10*). The rapid quench studies were carried out under single-turnover conditions using previously developed procedures (*10*). For holoTycB$_3$ATE, the deconvolution of adenylation, thiolation, and epimerization reactions starting from both L-Phe and D-Phe substrates was achieved (Figure 5). The microscopic rate constants and the apparent internal equilibrium constants for individual reaction steps catalyzed by holoTycB$_3$ATE starting from both L-Phe and D-Phe compared to holoGrsA reactions are listed in Table 3. The rates for both L-Phe and D-Phe reactions were largely reduced in the amino acid adenylation step and aminoacyl-S-Ppant-enzyme epimerization step compared to that of GrsA. For the L-Phe reaction, the holoTycB$_3$ATE was 470-fold slower in formation of the enzyme-bound L-Phe-AMP and 340-fold slower in L-Phe-S-Ppant-enzyme epimerization in comparison to the corresponding reaction steps catalyzed by holoGrsA. Similarly, 400-fold and 1000-fold reductions in rates were observed in adenylation and epimerization when D-Phe was

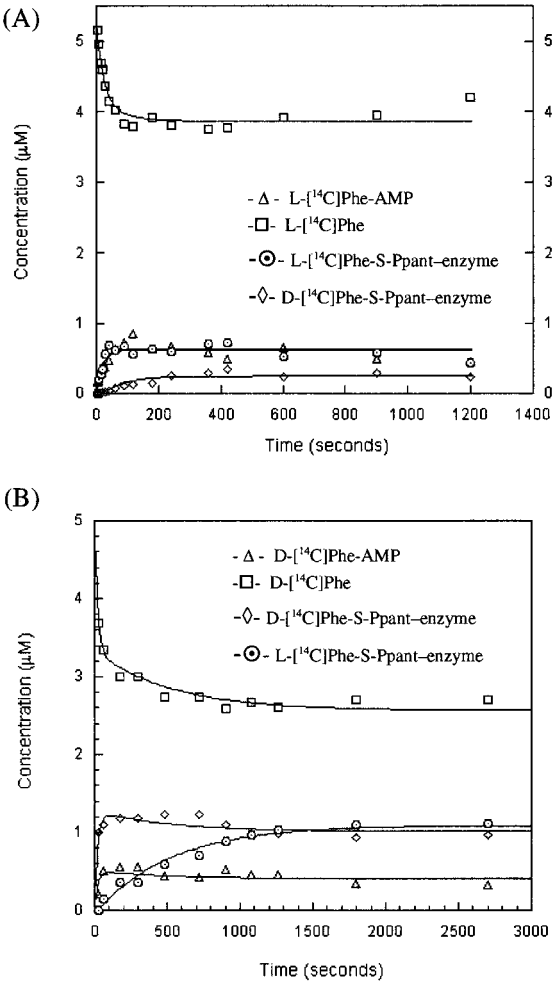

FIGURE 5: Time courses for the single-turnover reactions of 35 μM holoTycB$_3$ATE enzyme with 5 μM radiolabeled amino acid, 5 mM $MgCl_2$, 4 mM ATP, and 0.5 mM TCEP in 50 mM K^+Hepes (pH 7.5). (A) L-[^{14}C]Phe (□), L-[^{14}C]Phe-AMP (△), D-[^{14}C]Phe-S-Ppant-enzyme (◇), and L-[^{14}C]Phe-S-Ppant-enzyme (⊙). (B) D-[^{14}C]-Phe ([□]), D-[^{14}C]Phe-AMP (△), D-[^{14}C]-S-Ppant-enzyme (◇), and L-[^{14}C]-S-Ppant-enzyme (⊙) are shown with progress curves fitted by DYNAFIT.

Table 3: Comparisons of Rate Constants and Apparent Internal Equilibrium Constants for Individual Reaction Steps Catalyzed by HoloTycB$_3$ATE and GrsA Using L-[^{14}C]Phe or D-[^{14}C]Phe as Starting Substrates under Single-Turnover Conditions (See Experimental Procedures for Details)[a]

	k_1 (s^{-1})	k_{-1} (s^{-1})	k_2 (s^{-1})	k_{-2} (s^{-1})	k_3 (s^{-1})	k_{-3} (s^{-1})
GrsA[b] + L-[^{14}C]Phe	4.7	13	7.9	2.1	2.7	2.1
	$K_1^{app} = 0.36$		$K_2^{app} = 3.8$		$K_3^{app} = 1.3$	
GrsA[b] + D-[^{14}C]Phe	8 ± 2	39 ± 14	11 ± 1	1.0 ± 0.2	1.8 ± 0.4	2.5 ± 0.6
	$K_1^{app} = 0.21$		$K_2^{app} = 11$		$K_3^{app} = 0.7$	
HoloTycB$_3$ATE + L-[^{14}C]Phe	0.01	0.07	0.6	0.6	0.008	0.01
	$K_1^{app} = 0.14$		$K_2^{app} = 1$		$K_3^{app} = 0.8$	
HoloTycB$_3$ATE + D-[^{14}C]Phe	0.02	0.11	35	14	0.0017	0.0015
	$K_1^{app} = 0.18$		$K_2^{app} = 2.5$		$K_3^{app} = 1.1$	

[a] The apparent internal equilibrium constants were calculated from the ratio of microscopic rate constants. [b] GrsA results were reported in ref *10*.

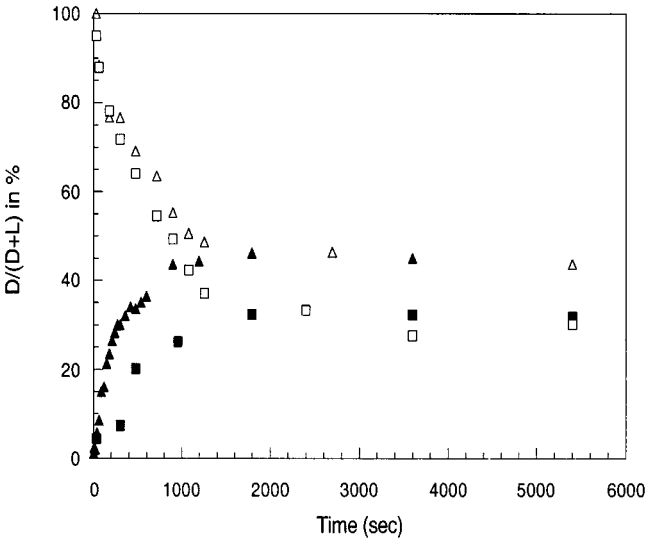

FIGURE 6: L-to-D and D-to-L conversion in the Phe-S-Ppant-T intermediate of holoTycB$_3$ATE (triangles) and holoTycB$_3$CATE (squares). Open symbols and closed symbols represent D-[^{14}C]Phe and L-[^{14}C]Phe as starting substrates, respectively.

used as the starting substrate for holoTycB$_3$ATE. For holoTycB$_3$CATE reactions, a slow hydrolysis of the covalent intermediate observed after 600 s prohibited us from obtaining the microscopic rates for all three steps accurately.

To investigate the extent of Phe-S-Ppant-enzyme epimerization in a time-dependent manner by holoTycB$_3$ATE and holoTycB$_3$CATE, we carried out single-turnover reactions to examine the ratio of L-Phe-S-Ppant-enzyme and D-Phe-S-Ppant-enzyme. The hydrolyzed products from the TCA precipitated enzyme pellet were analyzed by chiral TLC. The percentages of D-Phe in the total (D + L)-Phe over time are shown in Figure 6. The results revealed that the equilibrium position for holoTycB$_3$ATE was ca. 50% D-Phe whether the starting amino acid was L-Phe or D-Phe. In contrast, only about 30% of the overall Phe was in D-form at equilibrium starting from either L-Phe or D-Phe when holoTycB$_3$CATE was the catalyst. The obvious preference for L-Phe-S-Ppant-enzyme by holoTycB$_3$CATE at equilibrium agreed well with previous reports (*11*), supporting the hypothesis that the TycB$_3$C domain might enantioselectively bind and stabilize the L-form of Phe-S-Ppant-enzyme. It is noteworthy that the epimerization reactions by holoTycB$_3$ATE and holoTycB$_3$CATE were very slow compared to that by the GrsA E domain, suggesting that the internal E domain does not function very efficiently as an aminoacyl-S-enzyme epimerase.

D-Phe-Pro-L-Phe-SNAC and D-Phe-Pro-D-Phe-SNAC as Upstream (Donor) Substrate for HoloTycB$_3$CATE. The TycB subunit has three modules, encoding Pro$_2$Phe$_3$D-Phe$_4$ residues for transit to the five module TycC subunit. In the functioning tyrocidine assembly line, the donor substrate for the TycB$_3$C domain should be D-Phe$_1$-Pro$_2$-Phe$_3$-S-Ppant-T$_{TycB2}$ *in cis*. Since this complex natural tripeptidyl-T$_{TycB2}$ acyl-S-enzyme donor embedded within the three-module 10-domain TycB subunit was not available, we prepared D-Phe-Pro-L-Phe-SNAC as soluble surrogate peptidyl-thioester substrates, which simplifies the pantetheinyl-T$_{TycB2}$ scaffold to SNAC. This donor substrate in conjunction with L-[^{14}C]Phe-S-T$_3$ and D-[^{14}C]Phe-S-T$_3$ substrates *in cis* at the acceptor side allowed us to examine the TycB$_3$C domain substrate specificity at the acceptor side (Figure 7A).

The reactions containing 35 μM TycB$_3$CATE, 5 μM L-[^{14}C]Phe or D-[^{14}C]Phe, 4 mM ATP, 5 mM Mg^{2+}, and 0.5 mM of D-Phe-Pro-L-Phe-SNAC were acid quenched after specified periods of time (from 1 to 30 min). Any peptidyl-S-enzyme product was hydrolyzed by KOH treatment and released for chiral TLC and silica TLC analyses. Both TLC analyses revealed two new radiolabeled products formed over time in addition to the input L-Phe and D-Phe (see Figure 7B,C). The identity of the two tetrapeptide diastereomeric products was confirmed by comigration of synthetic standards D-Phe-Pro-Phe-L-Phe and D-Phe-Pro-Phe-D-Phe (data not shown). Tetrapeptide formation occurred about 9 min earlier for L-Phe than D-Phe reaction under the same reaction conditions, confirming an L preference for the TycB$_3$C domain at the acceptor side. The densitometric quantitation of the D-L-L-L- and D-L-L-D-tetrapeptides revealed near equal amounts of the tetrapeptidyl stereoisomers formed throughout the reaction, suggesting a pre-equilibrium epimerization on TycB$_3$.

To probe the upstream donor side selectivity, we compared two small-molecule analogues, D-Phe-Pro-L-Phe-SNAC and D-Phe-Pro-D-Phe-SNAC, as donor substrates when L-[^{14}C]-Phe-S-T$_3$ was serving as the acceptor side substrate (Figure 8A). No peptidyl-S-enzyme product was detected by TLC assay when D-Phe-Pro-D-Phe-SNAC was the donor, indicating an L selectivity at the donor side of the TycB$_3$C domain (Figure 8B&C).

Single-Turnover Characterization of HoloTycB$_{2-3}$ATCATE and the E Domain H1773A Mutant of TycB$_{2-3}$ ATCATE. Prior studies by Linne and Marahiel showed that elongation modules with the N-terminal C domain cannot initiate peptide bond formation (*11*). They therefore engineered a TycB$_{2-3}$ ATCATE construct lacking the N-terminal C domain. This initiation module (AT)−elongation module (CATE) mimic can catalyze Phe−Phe dipeptide formation and transfer it to the downstream module fused to a thioesterase domain (TycC$_1$CAT-Te) and generate the L-Phe-D-Phe-L-Asn tripeptide product. Hence, the six-domain TycB$_{2-3}$ ATCATE construct is a good candidate for detailed kinetic characterization of Phe−Phe dipeptide formation and epimerization. To further probe the stereospecificity of the TycB$_3$C domain at the acceptor side, we constructed H1773A TycB$_{2-3}$ ATCATE*. The mutation site was designed at the second histidine residue in the His motif (HHxxxDGxS) of the E domain (*17*). This His residue was shown to be a key catalytic residue for epimerization reaction in an initiation module E domain (His to Ala mutation in GrsA E domain impaired the interconvertion of the L-Phe- to D-Phe-S-Ppant-enzyme; *9*).

Single-turnover rapid quench analysis was carried out using holoTycB$_{2-3}$ATCATE and H1773A mutants in reactions with L-[^{14}C]Phe. The reactions were acid-quenched at specified times, and the radioactive species in the supernatant were separated from those in the protein pellet after centrifugation. The ^{14}C-labeled amino acid and aminoacyl-adenylate in the supernatant were analyzed by cellulose TLC. Separation of the hydrolytic products from covalent intermediates was accomplished by using two TLC analyses. The identities of the product peptides were confirmed by comigration with authentic peptide standards. As shown in Figure 9A, four covalent intermediates, L-Phe-, D-Phe-, L-Phe-L-Phe-, and L-Phe-D-Phe-S-Ppant-enzyme were observed in the

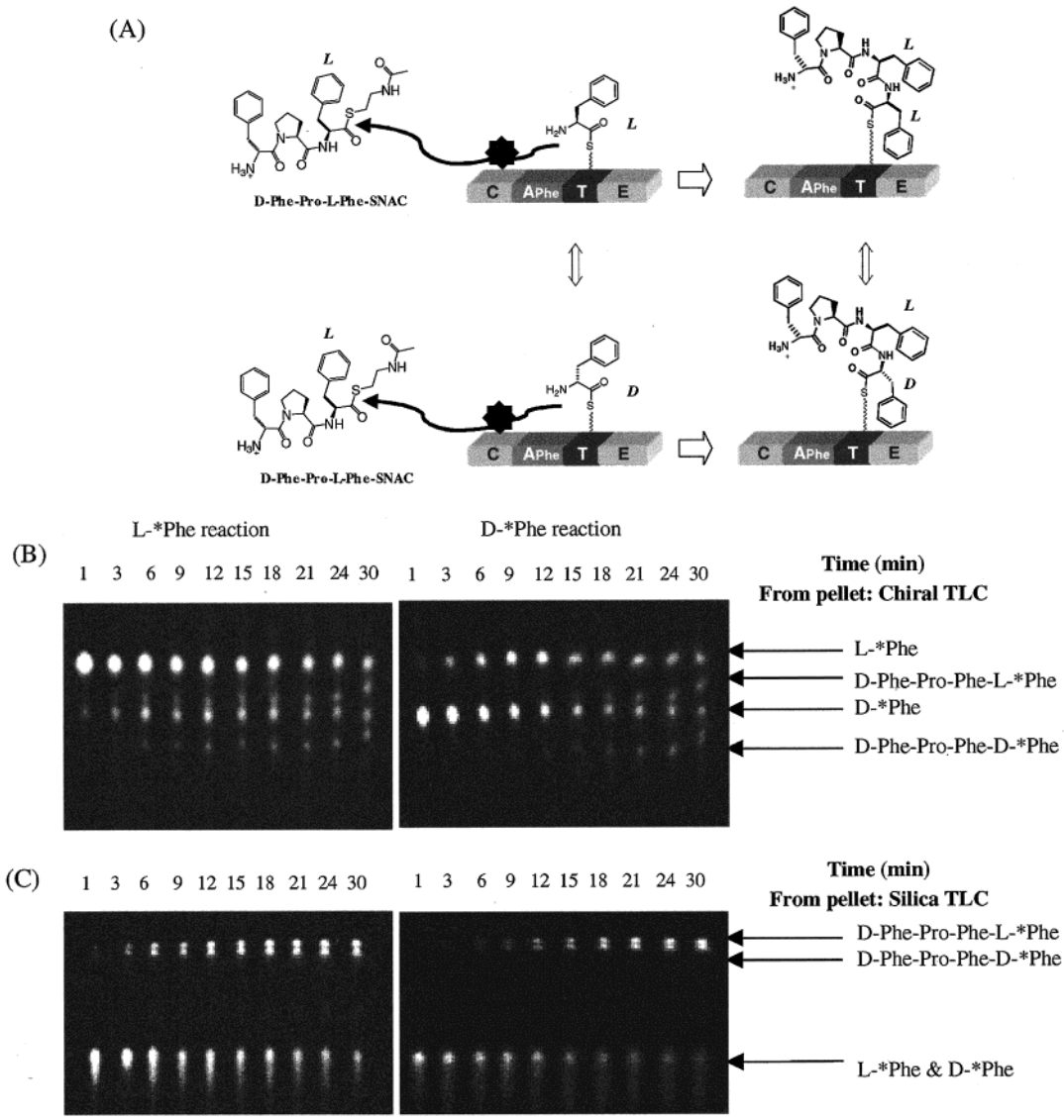

FIGURE 7: (A) Using D-Phe-Pro-L-Phe-SNAC to replace the D-Phe-Pro-Phe-S-Ppant-T domain for C domain acceptor specificity assay. The holoTycB$_3$CATE was reacted with L-[^{14}C]Phe or D-[^{14}C]Phe in the presence of D-Phe-Pro-L-Phe-SNAC. (B) Phosphorimages of the chiral TLC plate analysis of the single-turnover reaction products of 5 μM L-[^{14}C]Phe (left) and of 5 μM D-[^{14}C]Phe (right) reactions with 35 μM holoTycB$_3$CATE in the presence of 0.5 mM D-Phe-Pro-L-Phe-SNAC. (C) Phosphorimages of the silica TLC plate analysis of the single-turnover reaction products of 5 μM L-[^{14}C]Phe (left) and of 5 μM D-[^{14}C]Phe (right) reactions with 35 μM holoTycB$_3$CATE in the presence of 0.5 mM D-Phe-Pro-L-Phe-SNAC.

L-Phe reaction with holoTycB$_{2-3}$ATCATE. During the course of the reaction, the L-Phe-, D-Phe-, and dipeptidyl-S-Ppant-enzyme intermediates were formed *ad seriatim*. For H1773A and L-Phe reactions, only L-Phe-L-Phe but no L-Phe-D-Phe dipeptidyl product was formed (Figure 9B), confirming the prediction that the His1773 residue was essential for the epimerization of the dipeptidyl intermediate. The formation of L-Phe-L-Phe-S-enzyme product showed that the C domain can take L-Phe-S-enzyme as the downstream acceptor (Figure 9C).

To examine the C domain tolerance of D-Phe-S-T$_3$ as the acceptor substrate, we used D-Phe as the substrate to react with TycB$_{2-3}$ATCATE and H1773A. Since the two A domains in the bimodule construct can activate and load both L-Phe and D-Phe equally well, we cannot specifically load different stereoisomers to different modules. Instead, we addressed whether the TycB$_3$C domain could use D-Phe in both donor and acceptor positions loading both T$_2$ and T$_3$ domains with D-Phe. For D-Phe and TycB$_{2-3}$ATCATE reactions, D-Phe-, L-Phe-, D-Phe-L-Phe-, and D-Phe-D-Phe-S-Ppant-enzyme were all detected as reaction intermediates, albeit the rates were slower than those starting from L-Phe (Figure 10A). For the D-Phe reaction with the H1773A mutant, no dipeptidyl intermediate was formed over time (Figure 10B). This result suggested that the TycB$_3$C domain cannot accept D-Phe-S-T$_3$ as the downstream acceptor substrate. The D-Phe-D-Phe-S-enzyme formed in the wild-type reaction is thus likely to arise by the sequence D-Phe-T$_3$ $\leftrightarrow$ L-Phe-T$_3$ $\rightarrow$ D-Phe-L-Phe-T$_3$ $\rightarrow$ D-Phe-D-Phe-T$_3$ (Figure 10C).

From the single-turnover study results of TycB$_{2-3}$ATCATE and the H1773A mutant, a kinetic model for TycB$_{2-3}$ATCATE reactions with L-Phe was proposed (Figure 11). The time course of TycB$_{2-3}$ATCATE reactions with L-Phe was globally fitted to the kinetic models using the program DYNAFIT (*16*) and the progress curves shown in Figure 12. The two A domains in the TycB$_{2-3}$ATCATE construct both activate L-Phe. The deconvolution of any differences in rates of the adenylation and thiolation steps of these two

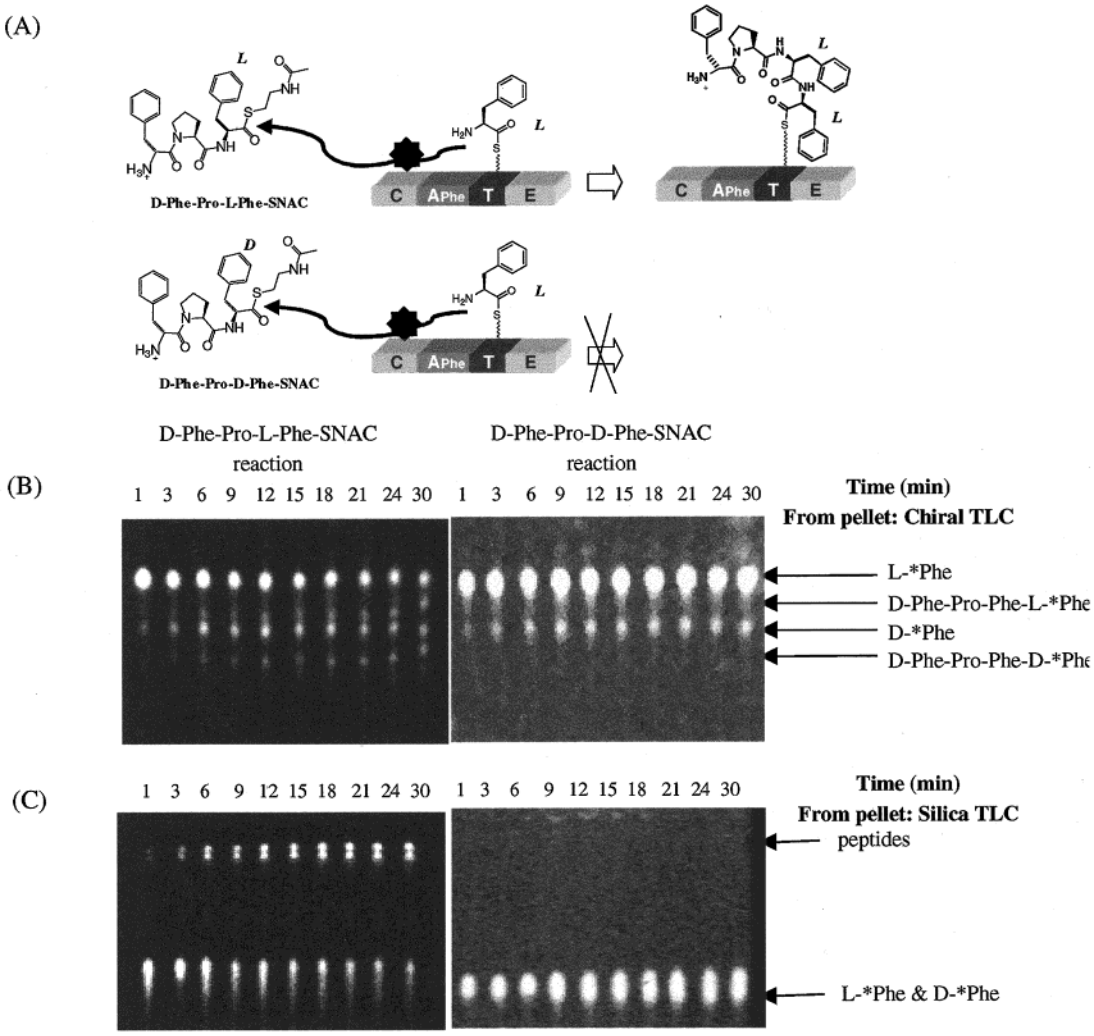

FIGURE 8: (A) Using D-Phe-Pro-L-Phe-SNAC and D-Phe-Pro-D-Phe-SNAC to probe the donor side substrate selectivity for $TycB_3C$ domain. The holo$TycB_3$CATE was reacted with L-[^{14}C]Phe in the presence of D-Phe-Pro-L-Phe-SNAC and D-Phe-Pro-D-Phe-SNAC. (B) Phosphorimages of the chiral TLC plate analysis of the single-turnover reaction products of L-[^{14}C]-Phe (5 μM) reactions with holo$TycB_3$-CATE (35 μM) in the presence of 0.5 mM D-Phe-Pro-L-Phe-SNAC (left) and 0.5 mM D-Phe-Pro-D-Phe-SNAC (right). (C) Phosphorimages of the silica TLC plate analysis of the single-turnover reaction products of L-[^{14}C]-Phe (5 μM) reactions with holo$TycB_3$CATE (35 μM) in the presence of 0.5 mM D-Phe-Pro-L-Phe-SNAC (left) and 0.5 mM D-Phe-Pro-D-Phe-SNAC (right).

L-Phe activating domains will require site-directed mutation to switch on and off each of the A and T domains in the two modules and analysis of the residual domains. In this study, we simplified this issue by proposing kinetic models assuming that the two A domains in $TycB_{2-3}$ATCATE behave similarly in adenylation and thiolation. The DYNAFIT fitting provided estimations of the microscopic rate constants and thermodynamic equilibrium constants for the five steps during the $TycB_{2-3}$ATCATE-catalyzed L-Phe reaction course (Table 4). Remarkably, the estimated rate of L-Phe-S-Ppant-enzyme epimerization was at least 3000-fold slower than that of the L-Phe-L-Phe-S-Ppant-enzyme epimerization, suggesting that the internal E_3 domain functions ca. 3 orders of magnitude better as a peptidyl-S-Ppant enzyme epimerase. In addition, the condensation reaction rate was estimated at $\sim$0.3 min^{-1}, comparable to the previously determined rate for the $TycB_1C$ domain to produce the Phe−Pro diketopiperazine, which is released from the Phe-Pro-S-Ppant dipeptidyl enzyme after the condensation reaction (formation at 1 min^{-1}) (*9*, *14*), allowing for pre-equilibration before transfer to the next downstream module. It is noted that the condensation reaction was significantly slower than peptidyl intermediate epimerization (200-fold in this model). This could be one of the strategies NRPS elongation domains employ to ensure the flux of the correct stereoconformer of the peptidyl intermediates through the assembly line.

DISCUSSION

Among the most challenging riddles of NRPS assembly line enzymology is the coordination and timing of the several steps that occur at each pantetheinyl-containing thiolation domain in every protein module as the chain grows, gets modified, and finally terminates. For example the 10-module tyrocidine synthetase includes 32 domains in the assembly line that carry out 33 chemical steps, not counting the phosphopantetheinyl priming of all 10 T domains. The assembly line must avoid premature hydrolytic termination of peptidyl-S-T domain intermediates and also avoid misinitiation at elongation modules. The peptide bond-forming C domains may be key gate keepers in flow control of tethered intermediates. The interplay of C domains and E domains examined in this study provides insight into when L-amino acid residues are epimerized to D-residues and how the timing and population of D-aminoacyl- versus L-aminoacyl-S-

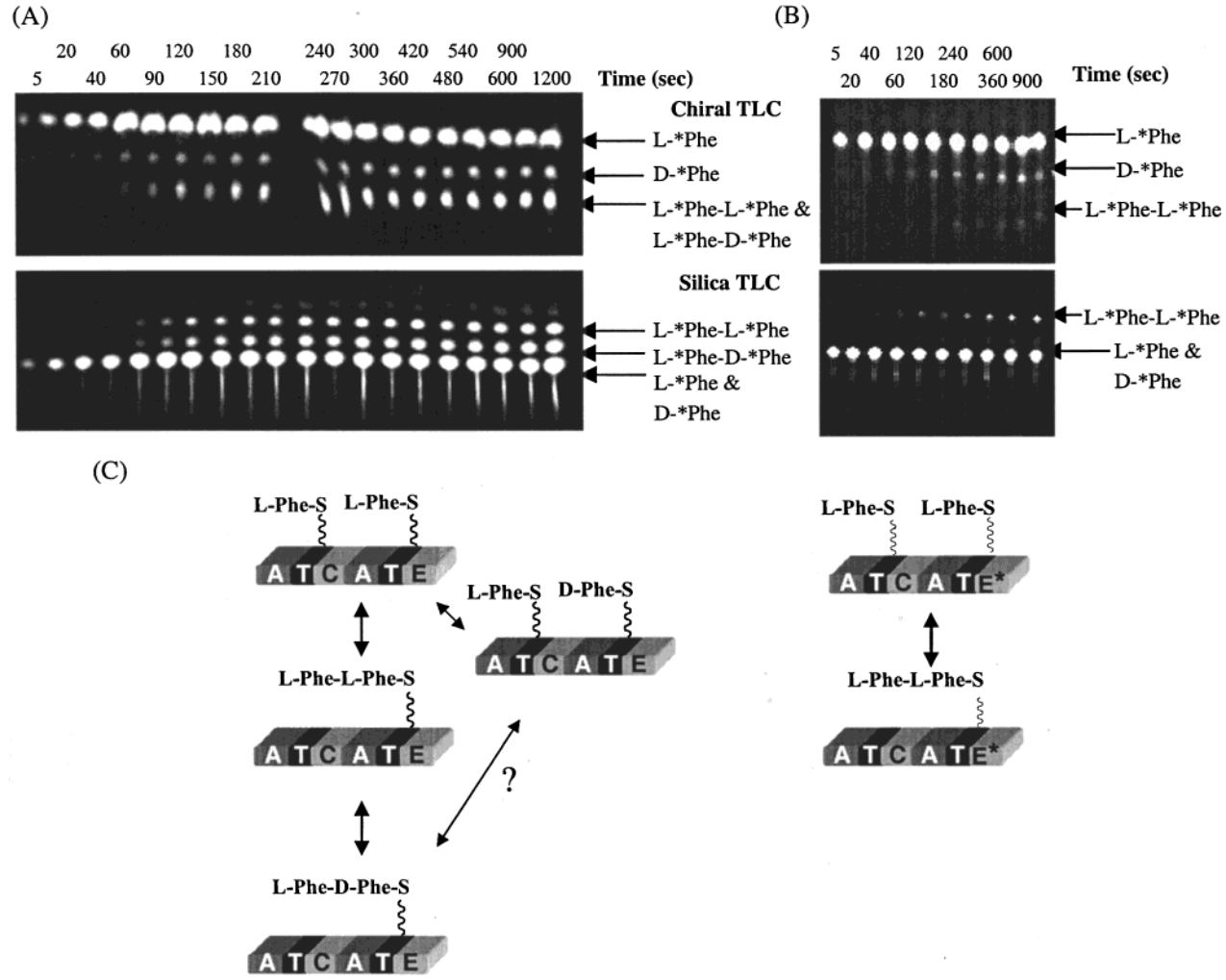

FIGURE 9: (A) Phosphorimages of the chiral TLC plate analysis (top) and silica TLC plate analysis (bottom) of the holoTycB$_{2-3}$ATCATE single-turnover reactions starting with L-[^{14}C]Phe. (B) Phosphorimages of the chiral TLC plate analysis (top) and silica TLC plate analysis (bottom) of the holoH1773A single-turnover reactions starting with L-[^{14}C]Phe. (C) Schematic representation of the dipeptidyl-S-enzyme formation by holoTycB$_{2-3}$ATCATE and holoH1773A(ATCATE*) in reactions with L-Phe.

enzyme intermediates and L-peptidyl- versus D-peptidyl-S-enzyme intermediates are dealt with by both upstream and downstream C domains to avoid stalling of chains that cannot be elongated.

D-Amino acid residues are signature elements of nonribosomal peptides (*5*, *18*), from penicillins to vancomycins to cyclosporin to bacitracin and tyrocidine (*2*, *19*, *20*). They can be incorporated by two routes. Free D-amino acids could be activated by A domains in the module responsible for incorporation for a given D-amino acid. This is quite rare, probably because of the low concentration of free D-amino acids in bacterial and fungal cells but is the case for D-Ala$_1$ incorporated by cyclosporin synthetase (*21*, *22*). A dedicated alanine racemase is encoded in that biosynthetic gene cluster (*21*). By far the most predominant route is to utilize available L-amino acid monomers of proteinogenic and nonproteinogenic amino acids (*5*, *6*) and epimerize them during incorporation/elongation. This C-α configurational equilibration is accomplished by 50 kDa E domains, acting locally within a module using aminoacyl-S-Ppant-T or peptidyl-S-Ppant-T as substrate *in cis*. To date, there has been no reported structure of an NRPS E domain, but there is homology to C domains, for which there is a recent structure (*23*).

Mechanistic analysis has been conducted on the initiation ATE module of gramicidin synthetase (*8*−*10*, *14*), which proved that the Phe-S-T thioester covalent enzyme intermediate was acted on by the E domain, presumably by a carbanion mechanism, and established that the D-Phe- and L-Phe-S-T intermediates were preequilibrated before the action of the downstream C domain. In contrast to the GrsA and TycA ATE initiation modules, most E domains in NRPS assembly lines reside in elongation modules. While the catalytic mechanism for epimerization is likely to be the same, the timing of epimerization to condensation might be different (as shown in Figure 2). In a prior study on actinomycin synthetase, it appeared that the dipeptidyl L-Thr-D-Val-intermediate formation proceeded through the L-Thr-L-Val-S-enzyme intermediate (*24*), suggesting the epimerization of the peptidyl intermediate. Initial studies on the TycB$_3$ module likewise indicated that the substrate for the internal E domain should be peptidyl-S-Ppant-enzyme (*11*).

To address the timing and identity of the epimerizing acyl enzyme species directly, we have analyzed the catalytic competence of the E domain of TycB$_3$ in rapid quench studies in the three-domain ATE and the four-domain CATE contexts. We then moved on to the bimodular ATCATE,

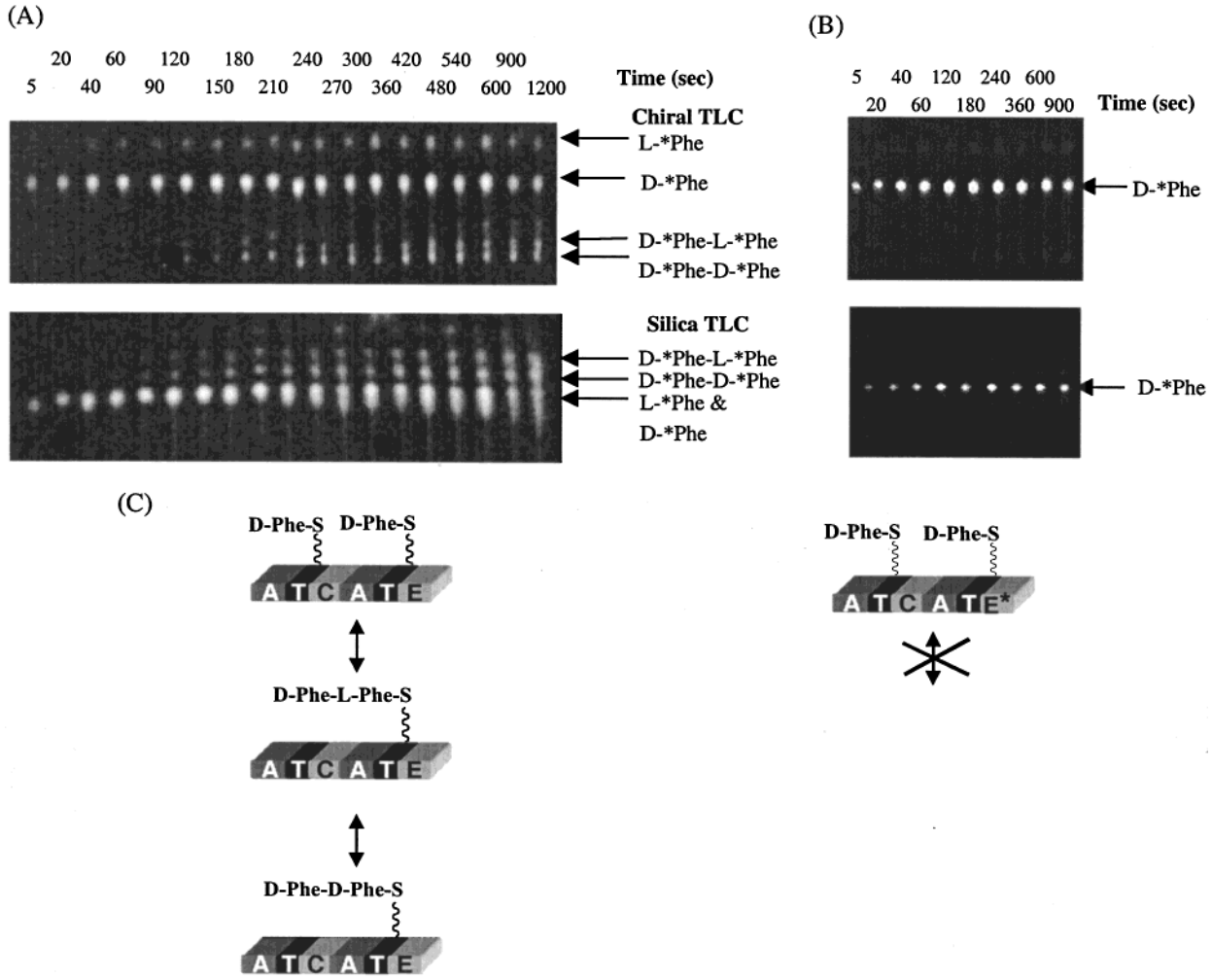

FIGURE 10: (A) Phosphorimages of the chiral TLC plate analysis (top) and silica TLC plate analysis (bottom) of the holoTycB$_{2-3}$ATCATE single-turnover reactions starting with D-[^{14}C]Phe. (B) Phosphorimages of the chiral TLC plate analysis (top) and silica TLC plate analysis (bottom) of the holoH1773A mutant single-turnover reactions starting with D-[^{14}C]Phe. (C) Schematic representation of the dipeptidyl-S-enzyme formation by holoTycB$_{2-3}$ATCATE and holoH1773A(ATCATE*) in reactions with D-Phe.

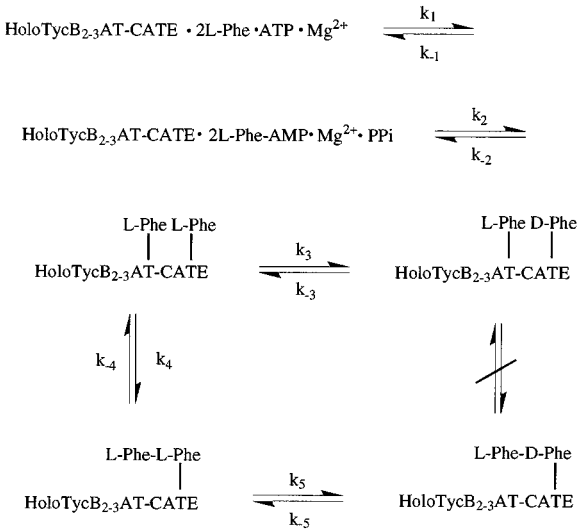

FIGURE 11: Kinetic models for holoTycB$_{2-3}$ATCATE-catalyzed dipeptide formation starting with the L-Phe substrate.

where one could measure both peptide bond formation and epimerization at the level of the aminoacyl-S-T or the dipeptidyl-S-T intermediate, coming from both the L and D directions. First we confirmed that the ATE fragment, while competent as a Phe-S-enzyme epimerase, was of quite low activity compared to the GrsA PheATE initiation module and the CATE four-domain version of the TycB$_3$ module. This could be due to some disruption of the A domain fold in the absence of the C domain since Phe-AMP formation rates are down some 60-fold. The CATE full TycB$_3$ module is nonetheless still very sluggish as a Phe-S-T domain epimerase (Table 3) in both L and D directions, down 200−1000-fold from the catalytic efficiency of the E domain of GrsA ATE (*10*). Linne and Marahiel (*11*) have previously shown that the ATE form of TycB$_3$ is competent as an initiation module while the CATE version is not, the C domain suppressing internal misinitiation, perhaps by sequestration of the phenylalanyl side chain. Indeed, a perturbation of the equilibrium from 50%/50% D-/L-Phe-S-T intermediate(ATE) to 30%/70% D-/L-Phe-S-enzyme (CATE) was observed, consistent with stereospecific sequestration of the L-Phe side chain by the C domain of Tyc B$_3$.

In the subsequent TycB$_{2-3}$ bimodule quench studies, we used ATCATE, rather than CATCATE, to enable chain initiation and production of a dipeptidyl Phe-Phe-S-T$_3$ enzyme and ascertain the timing of L-Phe-L-Phe versus L-Phe-D-Phe stereoisomer formation in competition with L-Phe-/D-Phe-S-enzyme formation. We were able to detect all four species after hydrolysis of the acyl enzyme forms and able

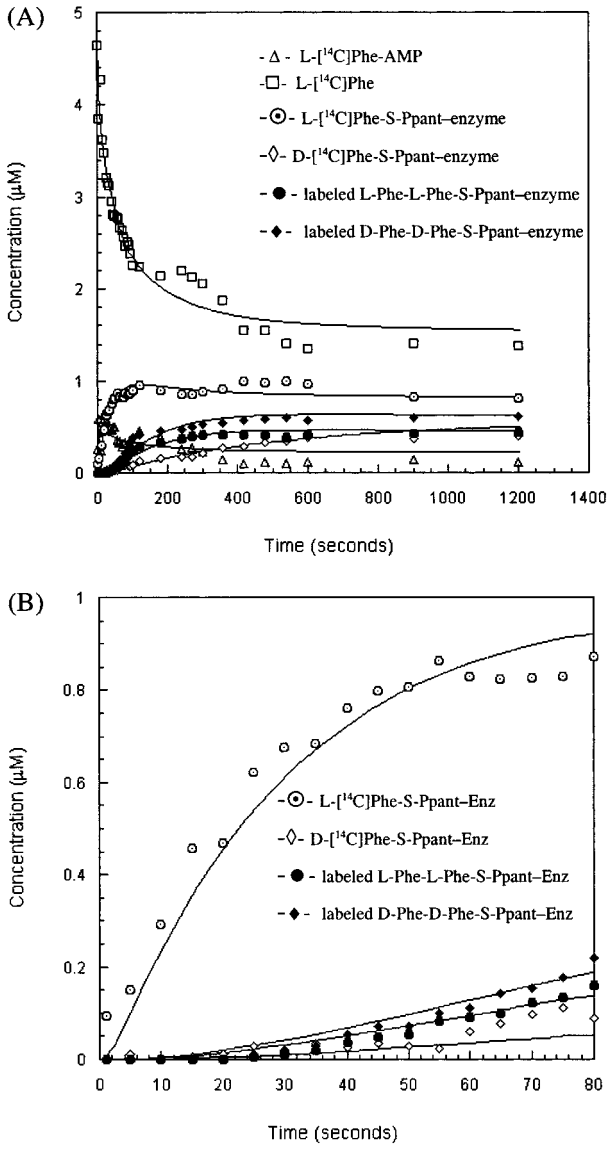

FIGURE 12: Time courses for the single-turnover reactions of 35 μM holoTycB$_{2-3}$ATCATE with 5 μM L-[^{14}C]Phe, 5 mM $MgCl_2$, 4 mM ATP, and 0.5 mM TCEP in 50 mM K^+Hepes (pH 7.5). (A) L-[^{14}C]Phe (□), L-[^{14}C]Phe-AMP (△), D-[^{14}C]Phe-S-Ppant-enzyme (◇), L-[^{14}C]Phe-S-Ppant-enzyme (⊙), L-[^{14}C]Phe-L-[^{14}C]Phe-S-Ppant-enzyme (●), and L-[^{14}C]Phe-D-[^{14}C]Phe-S-Ppant-enzyme (◆). (B) Blowup of the first 80 s of the same single-turnover reaction progress curve. For panel B, D-[^{14}C]Phe-S-Ppant-enzyme (◇), L-[^{14}C]Phe-S-Ppant-enzyme (⊙), L-[^{14}C]Phe-L-[^{14}C]Phe-S-Ppant-enzyme (●), and L-[^{14}C]Phe-D-[^{14}C]Phe-S-Ppant-enzyme (◆) are shown with lines from fitting.

to separate and quantitate the rates of aminoacyl and dipeptidyl-S-enzyme formation. The most striking result was that the bimodule was a much better dipeptidyl-S-enzyme epimerase than an aminoacyl-S-enzyme epimerase, strongly implicating that the D-Phe$_4$ configuration is not generated as the free Phe$_4$-S-enzyme but only after condensation, as the D-Phe$_1$-L-Pro$_2$-L-Phe$_3$-L-Phe$_4$-S-enzyme is epimerized only at Phe$_4$. This bimodule generates five covalent enzyme intermediates, and deconvolution of the rate constants for formation and decay of those five intermediates may have some errors due to simplifying assumptions that both A domains act equally on Phe substrates. But the conclusion of a 3000/1 kinetic preference for epimerizing the L-Phe-L-Phe-S-enzyme over the L-Phe-enzyme is likely to be on the correct order of magnitude.

We have previously noted that the chemical basis for the selective epimerization of the peptidyl-S-enzyme rather than the aminoacyl-S-enzyme with its free amino group could be an electronic one (*11*). The amino group lone pair is tied up in the peptide bond and will not provide electrostatic destabilization that the free amino group of the Phe-S-enzyme would provide to generation of the C_2 carbanionic transition state for epimerization. This could be the general mechanism for ensuring that peptidyl-S-enzymes are epimerized after condensation and may apply to all NRPS elongation modules that contain E domains.

These findings, if generalized from comparable indications in actinomycin synthetase and ACV synthetase (*24*, *25*), would make strong predictions about the stereoselectivity of C domains in NRPS modules for the peptidyl/aminoacyl side chains on both the upstream donor-S-T domain and the downstream acceptor-S-T domain. In particular, the C domain of TycB$_3$ should be $^{L}C_{L}$, where the superscript refers to the chirality for the upstream tripeptidyl donor (at Phe$_3$) and the subscript denotes the chiral preference for the downstream aminoacyl moiety (here Phe$_4$). The donor side selectivity was validated by comparison of two soluble donor substrates tripeptidyl D-Phe-L-Pro-L-Phe-SNAC and D-Phe-L-Pro-D-Phe-SNAC as donor molecules in the reaction with holoTycB$_3$CATE in the presence of L-[^{14}C]Phe. While D-Phe-L-Pro-L-Phe-SNAC was recognized by the TycB$_3$C domain as the donor and proceeded to form tetrapeptidyl-S-enzyme products, D-Phe-L-Pro-D-Phe-SNAC was not accepted by the TycB$_3$C domain, suggesting an L selectivity at the upstream donor side of the C domain. We validated the C domain chiral selectivity at the downstream acceptor side two ways. First, we switched off the E domain by mutation of His1773 and observed that the ATCATE* would take L-Phe-S-enzyme but not D-Phe-S-enzyme as the downstream acceptor substrate. Thus, in a dipeptidyl-S-enzyme-forming reaction, the C domain is L-specific. Second, we replaced the L-Phe$_3$ donor tethered on T$_2$ by D-Phe-L-Pro-L-Phe-SNAC in the presence of CATE and D- or L-[^{14}C]Phe. The L-[^{14}C]Phe reaction was significantly faster than the D-[^{14}C]Phe reaction. While the D-[^{14}C]Phe reaction did occur, it was likely going through a detour to form L-[^{14}C]Phe-enzyme intermediate first and then the formation of tetrapeptidyl-S-enzyme intermediate.

In previous studies, we showed that the TycB$_1$ module was accepting only the D-Phe-S-T$_1$ chain, not the L-isomer, and so was a $^{D}C_{L}$ version of a condensation domain in this

Table 4: Estimation of Rate Constants and Apparent Internal Equilibrium Constants for Individual Reaction Steps Catalyzed by TycB$_{2-3}$ATCATE Using L-[^{14}C]Phe as the Starting Substrate under Single-Turnover Conditions (See Experimental Procedures for Details)[a]

	k_1 (s^{-1})	k_{-1} (s^{-1})	k_2 (s^{-1})	k_{-2} (s^{-1})	k_3 (s^{-1})	k_{-3} (s^{-1})	k_4 (s^{-1})	k_{-4} (s^{-1})	k_5 (s^{-1})	k_{-5} (s^{-1})
HoloTycB$_{2-3}$ATCATE + L-[^{14}C]Phe	~0.09	~0.5	~0.08	~0.02	~0.0007	~0.0016	~0.005	~0.013	~2.3	~1.7
	$K_1^{app} = 0.2$		$K_2^{app} = 4$		$K_3^{app} = 0.4$		$K_4^{app} = 0.4$		$K_5^{app} = 1.4$	

[a] The apparent internal equilibrium constants were calculated from the ratio of microscopic rate constants.

assembly line (*26*, *27*). Prediction of the subsequent processing of the D-Phe$_1$-L-Pro$_2$-L-Phe$_3$-D-Phe$_4$-S enzyme intermediate by the next module, TycC_1 (see Figure 1), indicates this also will be a $^{D}C_{L}$ condensation domain. All the other six C domains in Tyc synthetase should be $^{L}C_{L}$. The molecular basis of chiral recognition of donor and acceptor aminoacyl side chains by C domains remains undetermined but has profound implications for domain and module swapping in NRP and NRP/PK hybrid (*3*) combinatorial biosynthetic schemes. Matching of E domains with their cognate upstream and downstream C domains may be required. By acting to epimerize the peptidyl-S-T intermediate rather than the aminoacyl-S-T intermediate in a T-E didomain pair, the E domains impose specific constraints on the two surrounding C domains where the upstream will be $^{L}C_{L}$ and downstream will be $^{D}C_{L}$. For example one predicts four $^{D}C_{L}$ condensation domains out of seven in the NRPS assembly lines that make vancomycin and teicoplanin.

Finally, if the C domains upstream and downstream of E domains will be chiral peptide synthetases with donor and acceptor stereospecificity as noted here, then the E domains must have a higher catalytic capacity than the immediate downstream C domains to avoid having peptidyl chains stall during chain growth because of incorrect stereochemistry. If the proximal residue of the peptidyl chain in the peptidyl-S-T covalent enzyme intermediates is epimerized at rates much faster than downstream peptide bond formation, then all the chains can be brought forward as D chains for elongation without kinetic barrier.

ACKNOWLEDGMENT

Dr. Susan Clugston is gratefully acknowledged for a careful reading of the manuscript.

REFERENCES

1. Schwarzer, D., and Marahiel, M. A. (2001) *Naturwissenschaften 88*, 93−101.
2. van Wageningen, A. M. A., Kirkpatrick, P. N., Williams, D. H., Harris, B. R., Kershaw, J. K., Lennard, N. J., Jones, M., Jones, S. J. M., and Solenberg, P. J. (1998) *Chem. Biol. 5*, 155−162.
3. Cane, D. E., Walsh, C. T., and Khosla, C. (1998) *Science 282*, 63−68.
4. Keating, T. A., and Walsh, C. T. (1999) *Curr. Opin. Chem. Biol. 3*, 598−606.
5. Marahiel, M. A., Stachelhaus, T., and Mootz, H. D. (1997) *Chem. Rev. 97*, 2651−2673.
6. Walsh, C. T., Chen, H. W., Keating, T. A., Hubbard, B. K., Losey, H. C., Luo, L. S., Marshall, C. G., Miller, D. A., and Patel, H. M. (2001) *Curr. Opin. Chem. Biol. 5*, 525−534.
7. Trauger, J. W., Kohli, R. M., Mootz, H. D., Marahiel, M. A., and Walsh, C. T. (2000) *Nature 407*, 215−218.
8. Luo, L. S., Burkart, M. D., Stachelhaus, T., and Walsh, C. T. (2001) *J. Am. Chem. Soc. 123*, 11208−11218.
9. Stachelhaus, T., and Walsh, C. T. (2000) *Biochemistry 39*, 5775−5787.
10. Luo, L., and Walsh, C. T. (2001) *Biochemistry 40*, 5329−5337.
11. Linne, U., and Marahiel, M. A. (2000) *Biochemistry 39*, 10439−10447.
12. Quadri, L. E. N., Weinreb, P. H., Lei, M., Nakano, M. M., Zuber, P., and Walsh, C. T. (1998) *Biochemistry 37*, 1585−1595.
13. Lambalot, R. H., Gehring, A. M., Flugel, R. S., Zuber, P., LaCelle, M., Marahiel, M. A., Reid, R., Khosla, C., and Walsh, C. T. (1996) *Chem. Biol. 3*, 923−936.
14. Stachelhaus, T., Mootz, H. D., Bergendahl, V., and Marahiel, M. A. (1998) *J. Biol. Chem. 273*, 22773−22781.
15. Ho, S. N., Hunt, H. D., Horton, R. M., Pullen, J. K., and Pease, L. R. (1989) *Gene 77*, 51−59.
16. Kuzmic, P. (1996) *Anal. Biochem. 237*, 260−273.
17. De Crecy-Lagard, V., Marliere, P., and Saurin, W. (1995) *C R Acad Sci III 318*, 927−936.
18. Vondohren, H., Keller, U., Vater, J., and Zocher, R. (1997) *Chem. Rev. 97*, 2675−2705.
19. Schofield, C. J., Baldwin, J. E., Byford, M. F., Clifton, I., Hajdu, J., Hensgens, C., and Roach, P. (1997) *Curr. Opin. Struct. Biol. 7*, 857−864.
20. Konz, D., and Marahiel, M. A. (1999) *Chem. Biol. 6*, R39−R48.
21. Weber, G., Schorgendorfer, K., Schneiderscherzer, E., and Leitner, E. (1994) *Curr. Genet. 26*, 120−125.
22. Dittmann, J., Wenger, R. M., Kleinkauf, H., and Lawen, A. (1994) *J. Biol. Chem. 269*, 2841−2846.
23. Keating, T. A., Marshall, C. G., Walsh, C. T., and Keating, A. E. (2002) *Nat. Struct. Biol.* (in press).
24. Stindl, A., and Keller, U. (1994) *Biochemistry 33*, 9358−9364.
25. Kallow, W., Neuhof, T., Arezi, B., Jungblut, P., and vonDohren, H. (1997) FEBS *Lett. 414*, 74−78.
26. Belshaw, P. J., Walsh, C. T., and Stachelhaus, T. (1999) *Science 284*, 486-489.
27. Ehmann, D. E., Trauger, J. W., Stachelhaus, T., and Walsh, C. T. (2000) *Chem. Biol. 7*, 765−772.

BI026047+